Non-Linear Optical Host-Guest Hybrid Material by Tight Confinement of LDS 722 into Aluminophosphate 1D-Nanochannels

Rebeca Sola-Llano, Virginia Martínez-Martínez, Yasuhiko Fujita, Luis Gómez-Hortigüela, Almudena Alfayate, Hiroshi Uji-i, Eduard Fron, Joaquín Pérez-Pariente, Iñigo López-Arbeloa

https://doi.org/10.1002/chem.201601736

Chem.Eur.J.2016,22,15700–15711

Non-Linear Optical Host-Guest Hybrid Material by Tight Confinement of LDS 722 into Aluminophosphate 1D-Nanochannels

Rebeca Sola-Llano,[a] Virginia Martínez-Martínez,*[a] Yasuhiko Fujita,[b] Luis Gómez-Hortigüela,[c] Almudena Alfayate,[c] Hiroshi Uji-i,[b] Eduard Fron,[b] Joaquín Pérez-Pariente,[c] Iñigo López-Arbeloa[a]

Abstract: In this work, hemicyanine dye LDS 722, is encapsulated into the 1-D elliptical nano-channels of MgAPO-11 aluminophosphate by crystallization inclusion method. The synthesis of the hybrid material has been optimized through a systematic variation of the crystallization conditions in order to obtain pure and large crystals (around 20 µm x 30 µm) suitable for optical applications. The tight fitting between the molecular size of the guest dye and the pore dimensions of the host has favored a rigid planar conformation of the dye, restricting its inherent flexibility, which is confirmed by molecular simulations. Consequently, the encapsulation of LDS 722 into MgAPO-11 has led to an astonishing enhancement of the fluorescence with respect to another analogous nanoporous aluminophosphate, MgAPO-5, with slightly larger cylindrical channels, and with respect to the dye in solution. Moreover, the perfect alignment of LDS 722 (dye with intrinsic non-linear-optical properties) along the channels of MgAPO-11 has revealed attractive second-order non-linear properties such as second harmonic generation, proven through microscopy measurements in single crystals.

Introduction

Non-linear optical (NLO) materials are of great interest due to their potential use in numerous disciplines such as in communication technologies, where many efforts are focused on the shift from electronic processes to an optical regime in order to transmit information with higher data rates while reducing the size of the devices.[1–3] Indeed, many useful photonic devices are based on NLO phenomena such as optical modulators, optical amplifiers, ultra-fast optical switchers, high-density optical data storage media, solid state lasers, etc.[4–6] Moreover, NLO properties are also widely applied in biomedicine research, particularly in fluorescence-based bioimaging and dynamic (photo)therapy applications, achieving larger penetration depths, less photo-toxicity and minimum background by two-photon excitation.[7]

Traditional NLO systems are based on inorganic crystals such as α-quartz, β-barium borate (BBO), monopotassium phosphate (KDP) or lithium niobiate ($LiNbO_3$), and semiconductors such as GaSe, offering the advantage of good mechanical and chemical stabilities; however, they are very expensive and require time-consuming fabrication processes.[8] As an alternative, organic NLO materials can reach much larger NLO efficiencies, faster responses, lower costs and are easy to process and integrate into optical devices.[9] Generally speaking, most organic π-conjugated molecules with strong electron donor and acceptor groups at the ends are promising compounds for NLO.[10,11] However, most of them tend to crystallize in centrosymmetric structures. The typical strategies developed to induce acentric molecular ordering include i) the rational design of molecular asymmetry for self-assembling in non-centrosymmetric organic crystals,[12] ii) orientation controlled by electrical poling of polymeric materials containing dipolar chromophores[13] or iii) a layer by layer deposition of NLO chromophores in films.[14] Nevertheless, these systems usually suffer from poor physicochemical stability and low hardness.

In recent times, the design and synthesis of a new class of advanced hybrid materials, metal–organic frameworks (MOFs), have gained interest in this sense as they are promising candidates for NLO materials, since they have revealed very high second harmonic generation (SHG) signals.[6,15,16] However, although new MOFs for NLO follow a synthetic strategy based on the use of chiral ligands, asymmetric ligands or mixed metal-connecting centers,[6,16,17] a clear correlation between their structure and the observed SHG efficiencies remain elusive. Instead, high second-order nonlinear optical activities have recently been demonstrated by the encapsulation of organic dipolar chromophores into an anionic 1D-MOF.[2,18] We should note here that the inclusion chemistry was successfully applied in microporous inorganic-host/organic-guest systems several years ago yielding interesting optical applications.[19-21] In this sense, the key for success is the synergy of the confinement effect of the organic dyes with good lasing and NLO properties (low pump threshold requirement, high efficiency, wavelength tunability) hosted into rigid inorganic molecular sieves with good intrinsic physical properties (mechanical, thermal, photo and chemical stabilities and optical transparency in the Vis-NIR radiation). Thus, a new generation of functional materials such as light-harvesting systems,[21–23] microlasers[24–26] and frequency converters[27,28a] based on the anisotropic alignment of dyes into zeolitic matrices with one-dimensional channels of molecular dimensions emerged.

Following this strategy, the inclusion of different non-centrosymmetric organic molecules, such as p-nitroaniline and analogous compounds, into different nanostructured hosts aimed at their SHG properties has so far mostly been performed via diffusional processes, i.e. by adsorption from the vapor phase or by cation-exchange from solution.[2,4,18,28a,29]. In those studies the authors proposed that the SHG effects are a direct result of the interactions between guests and hosts with polar properties, such as AlPO-5 and AlPO-11, but also high space restrictions within the channels will prevent the tendency of the molecular dipoles to dispose in opposite directions.[28] In this sense, the alternative approach, the crystallization inclusion method where the guest dye is occluded in the porous host during its crystallization, will allow a much tight fit between the molecular and channel dimensions[20,22,24,26], compared to diffusional post-synthesis methodologies. Thus, through a rational choice of the host structure with pores that perfectly match the size of a desired NLO organic guest, an extraordinary preferential alignment along the rigid inorganic channels could be achieved through the crystallization inclusion method and, as a consequence, interesting NLO properties could be envisaged. However, this method requires some particular considerations related to the organic dye to be used, which has to be soluble in the synthesis gel, stable under the hydrothermal synthesis conditions, and should not affect the synthesis of the final zeolitic structure.

In this context, hemicyanine-type dyes, which are aromatic compounds with a strong electron-donating group (amine) on one end of the chromophore and a strong electron-withdrawing group (pyridinium) on the other end connected by methylene groups, represent good candidates to be tightly confined within 1D-nanoporous hosts by crystallization inclusion. In this type of dyes, the emission takes place from an intramolecular charge transfer state (ICT),[30] and there is a great change in the dipole moment upon excitation, making them excellent candidates for NLO applications such as second harmonic generation (SHG) or two photon pumping (2PP) for the commonly used near-IR wavelengths 1064 nm and 800 nm. However, they are very flexible molecules and require very rigid environments to restrict their molecular motion in order to achieve high fluorescence or lasing efficiency;[31] indeed, rotational motions around the different bonds are responsible for the non-radiative deactivation, such as trans-cis isomerization, or especially the formation of twisted intra-molecular charge transfer (TICT) states, usually non-fluorescent.[32] In this sense, a tight confinement of these molecules in 1D-nanoporous hosts becomes crucial. Interestingly, hemicyanine dyes usually exhibit high solubility, and high thermal and chemical stability to withstand the severe conditions of the hydrothermal crystallization of the zeolitic nanoporous host.

Inspired by our previous studies about “one-pot” encapsulation of dyes with a molecular structure consisting of three fused aromatic rings, such as pyronine Y and acridine, into different 1-D nanoporous Mg-containing aluminophosphates (MgAPO),[20,22,33] in this work we report the crystallization inclusion of a hemicyanine dye, LDS 722 (see Figure 1), into MgAPO-11 (AEL structure-type) aluminophosphate, in an attempt to obtain highly fluorescent crystals with NLO properties. In this context, the “in situ” encapsulation of LDS 722 dye in a different framework, AlPO-5 (AFI structure-type), has been already reported demonstrating microlaser action in single crystals.[26] However although both frameworks are 1D and non-centrosymmetric structures (Figure 1), the cylindrical channels of AFI-structure are larger (7.3 Å in diameter) than the elliptical pores of the AEL-structure (4 x 6.5 Å) used in this work, which will lead to materials with strongly improved photophysical properties. Indeed, as will be shown below, the very tight fitting between the pore dimensions of MgAPO-11 (AEL) and the molecular size of the LDS 722 dye (2.5 x 4.9 x 18.6 Å) will render a hybrid material with a higher emission efficiency and important NLO properties, such as two-photon induced fluorescence and second harmonic generation, compared to the analogous 1D-host MgAPO-5 (AFI), which do not provide such a tight confinement of the dye, resulting in a material with poor fluorescence and NLO properties. A complementary molecular-simulation study will aid in understanding the experimental observations.

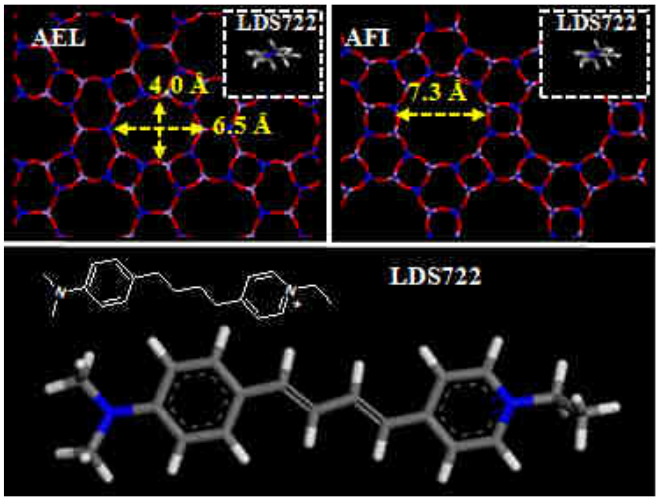

Figure 1. Structure and dimensions of the 1D-nanochannels of AEL and AFI frameworks compared with the section of LDS 722 (top), and molecular structure of LDS 722 (bottom).

Results and Discussion

Synthesis of LDS 722/MgAPO-11 hybrid material

As mentioned in the introduction, we followed the crystallization inclusion approach in our work. However, despite the simplicity of the "one-pot" synthesis previously optimized for MgAPO-11 crystals embedding cationic dyes structurally analogous to the anthracene ring with different substituted heteroatoms in one of the central CH groups, such as Pyronine Y and Acridine[20,22,33], the encapsulation of LDS 722 into MgAPO-11 through the same methodology was not such a direct task. In this case, our experimental observations showed that the LDS 722 dye molecule acts itself as a structure directing agent (SDA) towards the more favored MgAPO-5 (AFI). Indeed, the addition of LDS 722 into typical gels that would otherwise give pure MgAPO-11, led to the crystallization of MgAPO-5, and therefore we had to optimize the synthesis conditions in order to obtain pure LDS 722-containing MgAPO-11.

Table 1. Gel compositions: x MgO: 1 P_2O_5: (1-x/2) Al_2O_3: y EBA: z LDS 722: 300 H_2O and synthesis conditions (crystallization temperature, T) used in this work. The amount of dye loaded in the samples is expressed as grams of dye per 100 grams of solid product, and as percentage of the dye loaded with respect to the initial amount in the gel.

	x	y	z	T [ºC]	Phase[b]	mmol /100g	Dye uptake [%]
1	0.2	1	0.024	180	AFI+AEL(↓)	5.16	35
2[a]	0.2	1	0.024	180	AFI	8.70	71
3	0.2	1	0.008	180	AEL+AFI(↓)	1.32	27
4	0.2	1	0.008	195	AEL	0.88	18
5	0.2	0.75	0.008	180	AEL	0.60	15
6	0.2	0.75	0.008	195	AEL+ cristobalite	0.45	11
7	0.2	1.5	0.008	180	AFI+AEL(↓)	8.15	52
8	0.3	1	0.008	180	AEL+AFI	1.11	27
9	0.3	1	0.008	195	AEL+AFI	0.87	18
10	0.1	1	0.008	180	AEL+AFI(↓)	1.16	29
11	0.1	1	0.008	195	AEL*	2.20	44
12	0.1	1	0.016	180	AEL+AFI(↓)	3.60	43
13	0.1	1	0.016	195	AEL+AFI(↓)	3.60	43
14	0.1	1	0.024	180	AEL+AFI(↓)	8.47	59

[a] Sample under dynamic regime (agitation of the gel during hydrothermal crystallization); all other samples were prepared under static heating regime; [b] The main phase is denoted first and the minor phase in a second place; (↓) indicates a minor presence, and * indicates traces. (All XRD patterns of the powder samples are included in Figure S1 in the Supporting Information).

With this purpose, we have performed a systematic variation of the synthesis conditions, including the composition of the synthesis gel (Mg, structure-directing agent, SDA, ethylbutylamine in this case, and dye contents), crystallization temperature, crystallization time, and even crystallization regime. The most significant experiments are shown in Table 1. The starting point was the conditions used in our previous works to obtain pure MgAPO-11 loaded with Pyronine Y or Acridine[20,33] (sample 1 in Table 1); however, the addition of LDS 722 directed the crystallization pathway mainly towards MgAPO-5, evidencing that LDS 722 plays a particular and strong (taking into account its low concentration in the gel) structure-directing role towards the AFI framework. We attempted to obtain pure MgAPO-11 phases by using a dynamic crystallization regime, but instead a pure-MgAPO-5 phase was obtained under the same conditions (sample 2); we also observed that the crystallization time (from a few up to 48 hours) did not promote any effect on the phase selectivity. Hence, hereafter all samples were prepared through conventional static heating with a constant crystallization time of 24 hours.

We then studied the influence of the gel composition (Mg, ethylbutylamine used as SDA and dye contents) and the crystallization temperature, trying to find pure-phases of MgAPO-11 while achieving high amounts of encapsulated LDS 722 and high fluorescence efficiencies, both essential parameters for potential optical applications of these hybrid materials. Our first attempt was to decrease the dye content added in the gel from 0.024 to 0.008 (sample 3), trying to limit its AFI-structure-directing role; although still not pure, but a solid richer in MgAPO-11 was obtained, providing further confirmation that LDS 722 acts as a SDA towards MgAPO-5. In the next step, the temperature was increased from 180ºC to 195ºC (sample 4). In this case, we succeeded in producing a pure MgAPO-11 material; however, the amount of dye uptaken by the solid (0.88mmol/100g, only 18% of the dye added to the gel) was not high enough for optical applications (Figure 2). Such low incorporation of the dye might be associated to a competition between the SDA and LDS 722 molecules to get occluded within the AEL channels during the crystallization process.

In an attempt to increase the dye uptake, the SDA content of the gel was reduced (sample 5). However, although a smaller amount of SDA favored the crystallization of MgAPO-11 at 180ºC (compare sample 5 with sample 3 in Table 1), still only 15% of the dye in the gel was finally occluded in the solid (giving a total dye incorporation of 0.60 mmol/100g); a higher crystallization temperature led also to pure MgAPO-11 materials with low dye contents, although in this case the dense phase α-cristobalite also appeared in the final product (sample 6). Conversely, an increase of the SDA content (to 1.5) leads to MgAPO-5 (with a minor amount of MgAPO-11) at 180ºC (sample 7); we should note here that the dye uptake in the AFI phase is in general higher than in AEL (see Table 1).

Our next approach consisted of varying the Mg content in the gel. In principle, one would expect that higher Mg contents should enhance the incorporation of cationic molecules (being either protonated EBA or LDS 722) by inducing a higher negative charge population in the framework generated by the isomorphic replacement of Al3+ by Mg2+ in the inorganic host. An increase in the Mg content (to 0.3) (sample 8) rendered a mixture of MgAPO-11 and MgAPO-5, even at the higher temperature (sample 9). In contrast, by reducing the Mg content in the gel to 0.1 (sample 10), a MgAPO-11 material (with a minor amount of MgAPO-5) was obtained which contained almost twice the amount of dye, with a total dye content of 1.16 mmol/100g (equivalent to 29% of the added dye) (Table 1), compared to the material obtained with double amount of Mg in the gel (sample 5). Moreover, by increasing the crystallization temperature from 180ºC to 195ºC (sample 11), almost-pure MgAPO-11 was obtained (with only very minor traces of AFI), in which the amount of dye occluded was significantly increased, reaching a dye uptake yield of 44%, with a total dye amount of 2.2 mmol/100g (Table 1, Figure 2); this sample contains the highest amount of encapsulated LDS 722 in the AEL phase. This higher dye incorporation upon a decrease of the Mg content, and hence of the negative charge density in the framework, might be related to the smaller charge-density associated to LDS 722 compared to protonated EBA due to its larger size (with the same molecular charge).

In an attempt to further increase the dye loading within the MgAPO-11 material, a higher amount of dye (0.016) was added to the synthesis gel, and the synthesis was carried out both at 180ºC and 195ºC (samples 12 and 13). Results showed that the dye uptake did not change with the temperature. Interestingly, the increase in the dye content in the gel did increase its incorporation in the final solids (with respect to the materials obtained with a dye content of 0.008 in the gel), rising the dye loading in the AEL framework to 3.60 mmol/100g; it is remarkable that the dye uptake yield (with respect to the amount added to the gel) remained constant (43 %). We then further increased the molar concentration of dye in the gel to 0.024 (sample 14), yielding a MgAPO-11 material with the highest dye content found so far (8.47 mmol/100 gr, Figure 2). However, these samples prepared with higher dye contents in the gel (Samples 12, 13 y 14) showed a slightly higher presence of the AFI phase, though still in a minor amount. In conclusion, through this systematic variation of the synthesis conditions, several MgAPO-11 materials with different LDS 722 contents have been obtained.

In summary, in order to reach MgAPO-11 with high dye uptakes, the optimized gel composition should be 0.1 MgO: 1 P_2O_5: 0.95 Al_2O_3: 1 EBA: 0.008-0.024 LDS 722: 300 H_2O, undergoing the crystallization statically at 195 ºC for 24 hours.

General photophysical characterization

In general, hemicyanine dyes and particularly LDS 722 are very flexible molecules and they show very poor fluorescence emission efficiency in solution due to their free intra-molecular motions (vibrations, rotations and *cis-trans* isomerization) which drastically increase non-radiative processes and reduce the fluorescence. For this reason, one of the goals of this work was to increase significantly the emission capacity of LDS 722 by its encapsulation within the rigid elliptical nanochannels of AEL (4 Å x 6.5 Å) with adjusted dimensions with respect to the dye molecular size (2.5 x 4.9 x 18.6 Å).

Figure 2. Representative samples (4, 11 and 14) under ambient (top) and UV light (down).

Table 2. Dye loading of different samples and their main photophysical parameters together with those for the dye in solution: fluorescence quantum yield (Φ_{fl}), maximum emission wavelength (λ_{fl}) and fluorescence lifetimes (τ) after excitation at 530nm.

Sample	mmol /100g	Φ_{fl}	λ_{fl} [nm]	τ [ns]
solution	-	0.01	710	0.08
2 (AFI)	8.7	<0.01	~760	0.38
4	0.88	0.55[a] 0.18[b]	677	2.68
5	0.60	0.32[a] 0.13[b]	675	2.50 (79%) 0.6 (21%)
10	1.16	0.25[a] 0.13[b]	682	2.5 (88%) 0.6 (12%)
11	2.2	0.41[a] 0.20[b]	696	2.57
12	3.60	0.14[a] 0.09[b]	700	2.38 (62%) 0.67 (38%)
13	3.60	0.27[a] 0.19[b]	700	2.51 (84%) 1.12 (16%)
14	8.47	0.15[a] 0.12[b]	705	2.41 (67%) 0.80 (33%)

[a] Quantum yields registered under 410 nm excitation; [b] Quantum yields registered under 530 nm excitation.

LDS 722/MgAPO-11 samples show the typical broad red ICT emission band (Figure 3A) with a dramatic enhancement of the fluorescence efficiency. Fluorescence quantum yields recorded for the powder samples are two orders of magnitude higher than those in aqueous solution (Table 2). However, the inclusion of LDS 722 into the AFI structure, as previously reported by others,[26] with slightly larger channels, shows very poor emission comparable to that of the dye in solution (sample 2, Table 2).

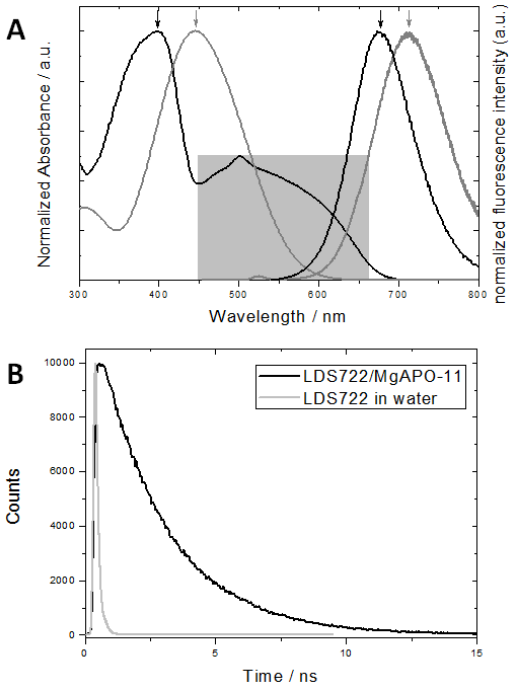

Figure 3. A) Absorption and emission spectra of the dye in aqueous solution (grey line) and LDS 722/MgAPO-11 powder sample (black line). B) Fluorescence decay curves registered for LDS 722 in aqueous solution (grey line) and within MgAPO-11 (black line).

Indeed, much longer lifetime values of around 2.5 ns registered for LDS 722/MgAPO-11 samples, compared to those of the dye confined in MgAPO-5 or in aqueous solution of several picoseconds (Figure 3B, Table 2), are a direct consequence of the decrease of the non-radiative pathways due to the confinement and rigidity imposed by the narrow channels of the inorganic AEL host. Moreover, the absorption and emission spectra of LDS 722/MgAPO-11 shows a hypsochromic-shift with respect to the dye in solution (Figure 3A, Table 2), which is also attributed to the strong confinement. Importantly, in the absorption spectra of LDS 722/MgAPO-11 samples, a new red-shifted band (highlighted as a grey square in Figure 3A) with respect to the main S_0-S_1 "locally-excited" ("LE") band is observed, which is assigned to the ICT state in the ground state. The planar configuration between D (donor) and A (acceptor) moieties not only facilitates the radiative emission from ICT state but also increases the molar extinction coefficient and broadens the ICT absorption spectra[10,34]. Indeed, higher quantum yields are obtained when the ICT excited state is directly populated by the excitation of ground state CT species, under green light at 530 nm, with respect to those registered upon excitation at the LE band, under UV-blue light at 410 nm (Table 2). Actually, at 410 nm excitation, a reminiscent emission band at around 450 nm ascribed to the radiative deactivation of LE is recorded together with the ICT emission band (Figure S2 in the Supporting Information).

These facts indicate that ICT in the excited state is not efficiently populated through relaxation from an excited LE state (Figure 4). Moreover, the excitation spectra (Figure S2), which differs from the absorption spectra (Figure 3A), showed the ground ICT band as the main responsible of the emission, in agreement with the aforementioned assumption.

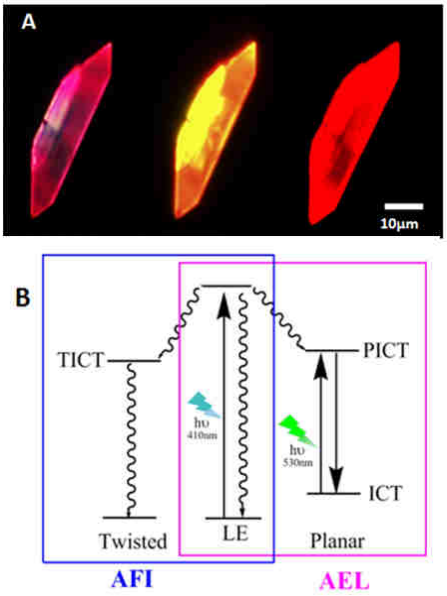

Figure 4. A) Emission images of a LDS 722/MgAPO-11 particle upon UV excitation light (with D350/50x band pass filter), blue light (with D470/40 band pass filter) and green light (with HQ530/30m band pass filter) excitations. B) Illustrative scheme of the electronic energy levels and the deactivation pathways of LDS 722 confined within the two different aluminophosphate frameworks.

The differences found in the fluorescence quantum yield of the samples (Table 2) recorded at the same excitation wavelength could be ascribed to the AFI impurities crystallized. The dye occluded in such structure does not practically show any fluorescence emission (Φ_{fl} < 0.01, Table 2) and consequently will decrease the absolute quantum yield of the powder sample. Indeed, in those samples with relatively lower quantum yields (i.e. samples 5 and 10 vs 4 and 11), a biexponential behavior is obtained from their respective fluorescence decay curves, τ_1 of around 2.5 ns previously attributed to LDS 722 in AEL, and a much shorter lifetime τ_2 of around 0.6 ns, indicative of a less rigid environment, probably LDS 722 in the AFI framework. Besides, there is a general drop in the fluorescence quantum yield as the dye loading in the MgAPO-11 samples increases: sample 4, with a dye content of 0.88 mmol/100g, shows a quantum yield of 0.55, compared to sample 14 with a dye loading 10 times higher but a quantum yield three times lower of 0.15 (Table 2, Figure 2). In optically dense materials, the most common problem usually arises from the formation of aggregates which usually quench the fluorescent emission of the monomeric species. However, the particular topology of the narrow channels of the AEL framework prevents any kind of aggregation. Instead, the red-shift up to 30 nm registered in the fluorescence bands of the more concentrated powder samples with respect to the diluted ones suggests the presence of reabsorption-reemission phenomena, that will be also responsible for the decrease of the fluorescence capacity in dye-concentrated samples (Figure 2). It is worth noting that, although those dyes whose emission takes place from ICT states usually show large Stokes shifts minimizing inner filters, the very probable ICT absorption band recorded for LDS 722 confined within the AEL framework enhances the possibility of reabsorption-reemission phenomena (Figure 3A).
Taking into account all these results, sample 11, with a considerable dye uptake and high fluorescence efficiency (Φ_{fl} = 0.41, nearly 40 times higher than that obtained for LDS 722 in aqueous solution), was selected as the best system for the characterization of NLO applications, as will be described below.

Molecular modeling

Our previous observations showed a much higher fluorescence of LDS 722 confined within the AEL framework compared to that observed when confined within the AFI framework and in solution. We applied molecular modeling techniques in order to understand this behavior by looking at the molecular confinement of LDS 722 in the different nanochannels.
We initially studied the location and stability of the LDS 722 isomers within the different MgAPO frameworks as a function of their isomerism. The coordinates of the Mg-containing AlPO frameworks were initially refined with GULP, using the potential by Catlow et al.[35] While there is only one unique T position in the AFI framework where Mg can replace Al, three possible locations are possible for the AEL framework, with Mg in T1, T2 or T3 (see Figure S3 in the Supporting Information).

Table 3. Interaction energy per molecule, relative energy of the different isomers and total interaction energy.

Framework	Mg position	Isomer	I. E.[a]	Rel. I. E.[b]
AFI	T1	LDS-trans	-151.9	0.0
		LDS-cis1	-142.7	9.1
		LDS-cis2	-135.8	16.1
AEL	T1	LDS-trans	-176.4	0.0
		LDS-cis1	-149.4	27.0
		LDS-cis2	-145.7	30.8
	T2	LDS-trans	-159.3	0.0
		LDS-cis1	-134.0	25.3
		LDS-cis2	-129.6	29.8
	T3	LDS-trans	-179.3	0.0
		LDS-cis1	-153.8	25.5
		LDS-cis2	-150.9	28.4

[a] In kcal/mol per molecule; [b] Compared to the most stable case, LDS 722-trans, in kcal/mol per molecule.

Then the different isomers (*trans*, *cis1* and *cis2*, see Figure S4 in the Supporting Information) of the LDS 722 molecules were loaded in the Mg-containing frameworks, and the most stable location and interaction energies were obtained by simulated annealing (Table 3). We analyze first results for the AFI framework. The incorporation of the *cis* isomers (*cis1* and *cis2*) is much less favorable than occlusion of the *trans* isomer (with relative energies of 9.1 and 16.1 kcal·mol^{-1} per molecule for *cis1* and *cis2*, respectively, with respect to the *trans* isomer). The low stability of the *cis*-isomers within the one-dimensional channels of the AFI framework is due to their molecular geometry, which deviates from the elongated shape of the *trans*-isomer that fits better within the cylindrical channels of the AFI structure (see Figure S5 in the Supporting Information for pictures). These results clearly suggest that only LDS 722-*trans* isomers are occluded within the AFI materials.

We then docked the molecules in the one-dimensional channels of the AEL framework, with an elliptical (rather than cylindrical as in AFI) shape and a slightly smaller aperture. Again energy results (Table 3) indicate that the cis-isomers do not fit well within these channels (see Figure S6 in the Supporting Information), being in this case even less favorable than in the AFI framework (with relative energies higher than 25 kcal·mol-1 per molecule); therefore, the possibility of having cis-isomers in the AEL framework is even smaller than in AFI. Only LDS 722-trans isomer will incorporate in the AEL materials. We docked this isomer with Mg in the three different positions, and found that the interaction energies were higher when Mg is located in positions 1 and 3 (Table 3); the interaction of the LDS 722-*trans* isomer with the framework when Mg is located in position 2 is much smaller, possibly due to the longer distance between Mg and the interacting atoms of the molecules (see Figure S7 in the Supporting Information). These results suggest that the most stable system involves Mg in position T1 or T3, developing a strong interaction with the LDS 722-*trans* isomer (Table 3).

Our next step was to analyze the flexibility of the LDS 722-*trans* isomers occluded within the different nanoporous frameworks in an attempt to understand the spectroscopic properties of the systems observed experimentally. Reduction of the fluorescence of LDS 722 can be caused by: i) *cis-trans* photoisomerization, process that may compete with fluorescence, which can be excluded since occlusion of *cis*-isomers is completely hindered, especially in the case of AEL, ii) deviation from the coplanar configuration between the donor and acceptor rings, being this coplanar configuration the one that activates the planar ICT (PICT) state, responsible of the fluorescence emission, and iii) rotation of the aniline group around the single C-N bonds, since these twisting motions allow the formation of a twisted ICT (TICT) state, a non-radiative state that efficiently quenches the fluorescence. In order to study both aspects, deviation of coplanarity (ii) as well as the torsion of the C-N bond (iii), 500 ps of NVT Molecular Dynamics of the LDS 722 molecules confined within both frameworks were run (at 298 K), and the statistical distribution of selected torsion angles during MD was analyzed (Figure 5-left) (see Figure S8 in the Supporting Information for definition of the torsion angles used). Deviation from coplanarity between the two rings is determined by the deviation of the torsion angle 1 (between the two aromatic rings) from 0º (which indicates a perfect coplanar configuration): large deviations of this angle from 0º involve a high flexibility of the molecule resulting in a large deviation from coplanarity, and consequently a lower fluorescence. The distribution of this torsion angle in the different systems (in a vacuum, in AFI and in AEL, Figure 5-top-left for the distribution) indicates a large deviation from 0º (given by the wide curve with wide tails) when the molecule is in a vacuum (blue line). Such deviation from 0º is only very slightly reduced when the molecule is occluded in the AFI framework, due to the large dimension (7.3 Å of diameter) and cylindrical nature of the nanochannels (red line) which does not impose a high constraintment on the molecule (Figure 5-right) (see Figure S9 in the Supporting Information for an example of deviation from coplanarity in AFI). In contrast, the angle distribution is much narrower, and the intensity around 0º is much higher, when the molecule is occluded within the AEL framework (green lines) for all the different Mg sites. This clearly indicates that deviation from coplanarity of LDS 722 is strongly prevented in the AEL framework

due to the elliptical shape of the nanochannels that impose a strong constraintment on the molecule (Figure 5-right), explaining the higher fluorescence observed for this system.

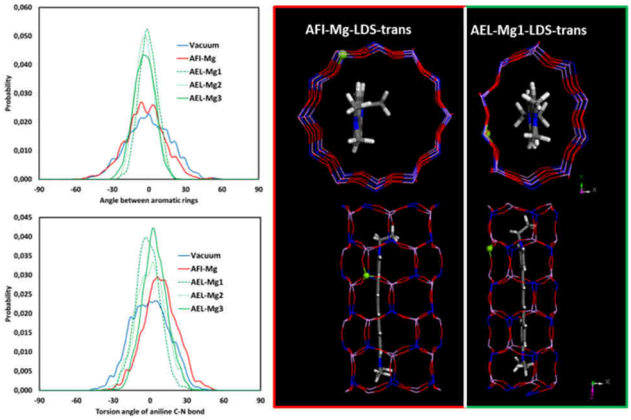

Figure 5. Left: Smoothed angle distributions between the aromatic rings (top) and of the C-N torsion angle of the aniline ring (bottom) of LDS 722-*trans* isomers in a vacuum (blue) or occluded within the Mg-AFI (red) or Mg-AEL (green, with different lines as a function of the Mg position). Right: Two views of the most stable location of the LDS 722-*trans* isomers within the one-dimensional (cylindrical or elliptical) channels of AFI and AEL frameworks.

We then studied the other possible source of fluorescence deactivation, the rotation of the C-N bond of the aniline ring; the distribution of the C-N torsion angle is plotted in Figure 5 (bottom-left). Again we observe that the torsion distribution is broad for the LDS 722 molecule in a vacuum (blue line), suggesting that this bond is able to rotate. Such C-N rotation is slightly prevented when the molecule is hosted in the AFI framework (red line), and is strongly impeded when the host is the AEL framework (especially in the most stable 1 and 3 Mg positions), again a consequence of the more tight confinement provided by the smaller elliptical channels of this structure. Our simulations thus clearly explain the better fluorescence properties of LDS 722 occluded within the AEL framework in terms of a prevention of the *cis*-photoisomerization, deviation from coplanarity and C-N bond rotation because of the tight confinement provided by the AEL host.

Non-linear Optical Applications

As previously mentioned, sample 11 was selected for the further study of NLO properties. As has been demonstrated above, the tight encapsulation of LDS 722 into the 1D-rigid nanopores of the AEL structure has led to an extraordinary enhancement of the fluorescence. On the other hand, with the aim of achieving a material with Non-Linear Optical properties, a non-centrosymmetric disposition of the molecules with the molecular dipoles pointing in the same direction within the AEL channels is required.

The alignment of the dye along the channels is qualitatively provided by the fluorescence dichroic ratio, 'D'. Large D values indicate a high degree of dye molecules in a preferential order[36]. Indeed, a huge anisotropic response to the linear polarized light is derived in this material (see Figure 6), providing dichroic ratios higher than 50 which represent, to our knowledge, the highest value found so far[20,33,36]. This feature, together with the fact that the LDS 722 dye shows intrinsic NLO properties, makes our hybrid material potential for Second-Order Non-Linear Optical properties such as Second Harmonic Generation and two photon induced fluorescence.

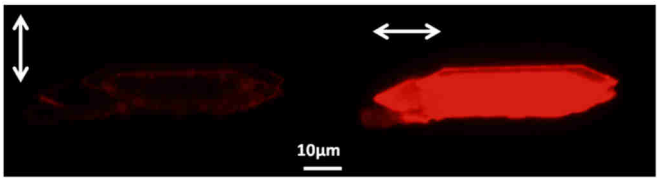

Figure 6. Polarized fluorescence images of LDS 722/MgAPO-11 particles under green excitation light. Arrows indicate the direction of the polarized light.

To study non-linear optical properties, polarized-fs laser light is focused to single crystals of sample 11. Figure 7A shows the emission spectrum recorded when focusing the incident laser light (excitation wavelength: 1024 nm, power: 0.1 mW) to the center of a sample 11 crystal (black curve) and of a blank crystal without dyes (green curve), deposited on a cleaned cover slip. The spectrum shows a sharp peak at 512 nm and a broad band centered at around 650 nm; note here that the polarization angle of incident light in all the experiments was set parallel to the transition dipole moments aligned along the AEL nanopores. This polarization orientation was confirmed by systematically rotating light polarization of the incident light and was set to the angle giving maximum fluorescence intensity (see Figure S10 in the Supporting Information for a detailed procedure). Furthermore, both the sharp and broad peaks show a quadratic power dependence (as shown in Figure S11 in the Supporting Information). Given

the strong polarization effect and the quadratic power dependence, we assigned the sharp and the broad peaks to be SHG and 2-photon excited fluorescence. Note also that immersion oil was dropped on the cover slip, in order to reduce 'undesirable' SHG contribution from crystal-glass or crystal-air interface as much as possible. Indeed, no peak was observed when the laser is focused on the cover slip, indicating that SHG contribution from glass-oil interface itself can be neglected. The spectrum of the sample 11 crystal shows a clear SHG peak with respect to the blank crystal that did not show any significant contribution at this excitation power (Figure 7B). This result likely indicates that the SHG signal is generated not from the framework itself but from the dyes distributed inside the crystal. In order to confirm this, the intensity of the laser light was significantly increased to induce photobleaching of the dyes, and the spectrum was continuously recorded over time during the laser irradiation (Figure 7C). Both SHG and 2-photon fluorescence intensities decreased significantly over laser irradiation due to a photobleaching of the dyes, whereas SHG intensity of the blank crystal did not show any notable decrease (Figure 7D) even at a higher laser power (> 10 mW). Note here that although blank crystals start showing SHG contribution above the excitation power around 1 mW (Figure S12 in the Supporting Information), its intensity is more than 100 times weaker than that on the sample 11 crystal.

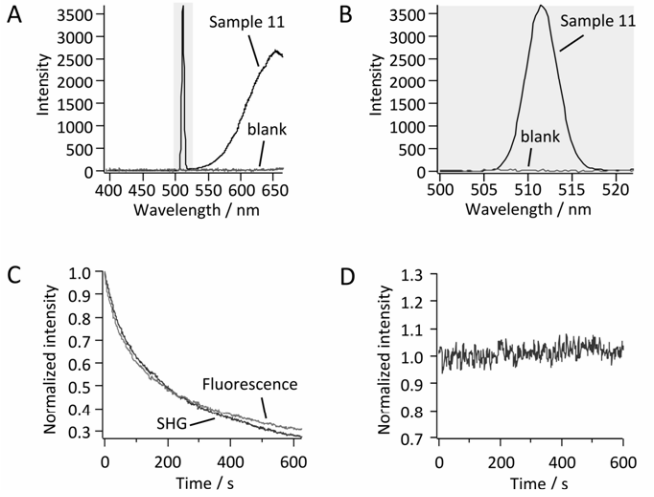

Figure 7. A) SHG/2-photon fluorescence spectrum recorded for sample 11 and SHG spectrum for blank crystals observed at 1024 nm excitation wavelength with 0.1 mW excitation power. B) Enlarged image of the SHG signal centered at 512 nm. C) Time dependence of SHG and fluorescence signals (normalized at 0 s exposure) of sample 11 excited at 812 nm with 2.4 mW excitation power. D) Time dependence of SHG intensity (normalized at 0 s exposure time) of the blank crystal excited at 1024 nm with 12 mW power.

In this regard, it is important to note here that in order to achieve a hybrid material with SHG properties, the guest dye, LDS 722 in the present case, should have intrinsic Non-Linear Optical properties (π-conjugated molecules with strong electron donor and acceptor groups) because our previous materials reported in earlier works based on the encapsulation of other dyes such as acridine (AC) and pyronine Y (PY) into MgAPO-11[20,33] also provided highly fluorescent hybrid systems with an extraordinarily-preferential alignment of the chromophores, but did not give almost any second harmonic generation response (Figure S13 in the Supporting Information).
In order to study the wavelength tunability of our hybrid material and identify the most efficient excitation wavelength to generate/excite SHG/fluorescence, the excitation wavelength of the laser light was tuned from 812 to 1222 nm (Figure 8A) at the same laser power (variations of laser power between wavelengths are corrected within 6 %) set at 0.1 mW in order to minimize photobleaching of the dye and to avoid any SHG contribution from the framework itself. Figures 8B and 8C, respectively, show intensity plots of SHG and 2-photon fluorescence as a function of the excitation wavelength. We found that, although SHG and 2-photon fluorescence peaks are observed for all excitation wavelengths, maximum intensities of both SHG and 2-photon fluorescence were found at excitation wavelengths in the region 1000-1020 nm. In this regard, we can conclude that both SHG and 2-photon processes occur with the highest efficiencies upon excitation with fs pulses in the range of 1000-1020 nm.

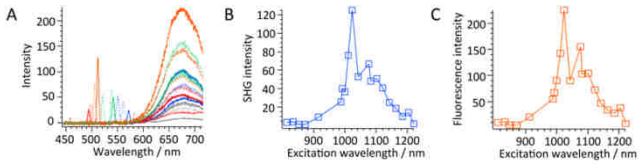

Figure 8. A) SHG/fluorescence spectra B) SHG intensity and C) 2-photon fluorescence intensity at different excitation wavelengths from 812-1222 nm with 0.1 mW excitation power. The measurements were carried out exciting a sample 11 crystal.

Conclusions

The encapsulation of the very flexible hemicyanine dye LDS 722 within the rigid elliptical nanochannels of AEL (4 Å x 6.5 Å), with adjusted dimensions with respect to the dye molecular size (2.5 x 4.9 x 18.6 Å), has significantly increased the emission capacity of LDS 722 at least by two orders of magnitude ($\Phi_{fl} > 0.40$) with respect to the analogous 1D-host MgAPO-5 (AFI), with slightly larger cylindrical channels with a diameter of 7.3 Å, or with respect to the dye in solution ($\Phi_{fl} \leq 0.01$). The high constraintment imposed by the AEL framework to LDS 722 has greatly restricted its molecular motion (free rotation of the C-N bond of the aniline ring) and prevented a deviation from coplanarity, both effective quenching paths of the fluorescence.
Due to the intrinsic NLO properties LDS 722 dye disposed in an extraordinary non-centrosymmetric alignment along MgAPO-11 channels, the final hybrid material has rendered SHG and 2-photon fluorescence signals under excitation wavelengths in the 812-1222 nm, being the most efficient excitation wavelength between 1000-1020 nm. Our work represents a clear proof of how fundamental is a perfect matching between the molecular size of a NLO dye guest and the pore dimensions of a rigid 1D-framework host in order to impose a collective alignment of the dye molecules with its molecular dipoles pointing in a preferred direction along the macroscopic crystal that can only be achieved via the crystallization inclusion approach.

Experimental Section

Synthesis of MgAPO materials. Mg-containing aluminophosphates (MgAPO-5 and MgAPO-11) were prepared using phosphoric acid (Aldrich, 85 wt%), magnesium acetate tetrahydrate (Aldrich, 99 wt%,), aluminium hydroxide (Aldrich), ethylbutylamine (EBA, Aldrich) and LDS 722 dye (Exciton, laser grade, used as received with a purity > 99%, checked by spectroscopic and chromatographic methods). The gels have a general molar composition of: x MgO: 1 P_2O_5: (1-x/2) Al_2O_3: y EBA: z LDS 722: 300 H_2O, where 'x' was varied between 0.1 and 0.3, 'y' between 0.75 and 1.5 and 'z' between 0.008 and 0.024; pH of the synthesis gels was between 4 and 5. The gels were heated under autogenous pressure. The solid products were recovered by filtration, exhaustively washed with ethanol and water and dried at room temperature overnight. In this work, the synthesis conditions, including the composition of the synthesis gels, as well as the crystallization time and temperature, were optimized in order to get pure samples of LDS 722-containing MgAPO-5 and MgAPO-11 materials.
Characterization. X-ray powder diffraction (XRD) was used to determine the crystalline phase obtained; XRD patterns were collected with a Panalytical X'Pro diffractometer using Cu Kα radiation. The dye content within the solid products was determined photometrically using a double beam Varian spectrophotometer (Cary 7000), after dissolving the solid material in 5 M hydrochloric acid and comparing the resulting solutions with standard solutions prepared from known concentrations of the dyes at the same pH value of the sample solutions (more details in the Supporting Information, Figure S14).
The absorption spectra of the LDS 722/MgAPO powder samples were recorded with a Varian spectrophotometer (model Cary 7000) detecting the reflected light by means of integrating sphere. The respective spectra of the MgAPO powders synthesized under identical conditions but without dyes were recorded and subtracted from the sample signal to eliminate the scattering contribution to the absorption spectra. Emission spectra of the powder were recorded in an Edinburgh Instruments spectrofluorimeter (FLSP920 model) in front-face configuration (40° and 50° to the excitation and emission beams, respectively) and leaned 30° to the plane formed by the direction of incidence and detection. The fluorescence lifetime decay curves of the bulk powder were measured with the time correlated single-photon counting technique in the same spectrofluorimeter using a multichannel plate detector (Hamamatsu R38094-50) with picosecond time-resolution (~20 ps). Fluorescence decay curves were monitored at the maximum emission wavelength after excitation by means of a Fianium Supercontinuum laser at 530nm with 150 ps full width at half maximum (FWHM) pulses. The fluorescence lifetime (τ) was obtained after deconvolution of the instrumental response signal from the recorded decay curves by means of an iterative method. The goodness of the exponential fit was controlled by statistical parameters (chi-square, χ^2, and analysis of the residuals). Absolute photoluminescence quantum yield of the LDS 722/MgAPO powders were measured in an integrated sphere coupled to this spectrofluorimeter. The absorbance at the excitation wavelength was obtained by comparing the scatter signal of the dye-loaded hybrid material and a Teflon disk used as a reference (with a diffuse reflectance of 100%).
Fluorescence images were recorded with an optical inverted microscope with epi configuration (Olympus BX51) equipped with a color CCD camera (DP72, Olympus). Crystals were excited under UV light, blue light and green light by respective Chroma band pass filters (D350/50x, D470/40 and HQ530/30m, respectively) and the emission was collected with Chroma cut-off filters (E400LPv2, E515LPv2 and E580lp, respectively). For polarized emission images, a polarizer (U-AN-360-3) was inserted before the detection of the image on the CCD camera. Fluorescence spectra of particles were recorded using an Edimburgh Instruments spectrofluorimeter (model FLSP920) coupled to the Olympus microscope via an optical fiber.
Fluorescence single-particle measurements were performed in a time-resolved fluorescence confocal microscope (model Micro Time 200, PicoQuant). The excitation was performed at 470 nm with picosecond pulsed diode lasers (PicoQuant, LHD 470 model) with 100 ps pulses at 5 MHz repetition rate. The fluorescence signal was collected by the same objective and focused (via a 50 μm pinhole) onto avalanche photodiode detectors (Micro-Photon-Devices MPD-APD). Polarization measurements were performed with unpolarized excitation light and the emission was collected by a polarizer beam splitter that divides the signal into two mutually perpendicular polarization orientation beams that were simultaneously detected by two detector channels. We

analyzed the dichroic ratio ('D'), defined as the relation between the emission-intensity counts collected for two perpendicularly polarized radiations.

NLO measurements. An ultrafast Ti:sapphire laser (Maitai-SP, SpectraPhysics) was used to generate the 820 nm pulses, 120 fs pulse duration (repetition rate 80 MHz). The laser beam was split into two paths with ratio of 9:1. The stronger beam was guided to an optical parametric oscillator (OPO) (Inspire HF200, SpectraPhysics) and used to generate the 940-1222 nm pulses. The polarization of the 820 nm pulses was controlled by a half-wave plate. Each beam was reflected by dichroic mirror (z750spxrxt, Chroma) after passing through a longpass filter (HQ800LP, Chroma) in order to reflect stray light generated from OPO, and then was focused to samples using an objective (PlanApo N.A. 0.95, x60, Nikon). With this configuration, a wide range of photon flux was available at the sample position. Considering a pulse average power of 0.5 mW at 1180 nm, a minimum nr of 1.88 x 1015 photons/(pulse x cm^2) is obtained while for a pulse with an average power of 10 mW at 820 nm a nr of 6.41 x1016 photons/(pulse x cm^2) could be achieved. The availability of such a wide range is important for the laser power dependent experiments (vide infra) where the probability of having one or two photons arriving at the sample at the same time is of key importance in investigating nonlinear processes. Substrates were mounted on a three-axis piezoelectric stage (P-517.3CL, Physik Instrumente, PI) equipped on an inverted microscope (TiU, Nikon). SHG and fluorescence signals from crystals were collected by the same objective, and then transmitted through a short-pass filter (ET750SP-2P, Chroma) to remove the excitation light. The light was focused onto the entrance slit of a spectrograph (iHR320, Horiba), and detected by a cooled-charge coupled device (CCD) (Newton 920, Andor).

Computational details. The computational methodology employed to study the occlusion of LDS 722 within the AFI and AEL frameworks was based on molecular mechanics simulations, as implemented in Forcite module in Materials Studio software[37]. The geometry of the zeolite structures were taken from the Material Studio database. Molecular structures and the interaction energies of the LDS 722 molecules with the framework are described with the CVFF forcefield[38]. A careful selection of the atom-types in this force-field ensures a proper model of the molecule, giving molecular structures of LDS 722 in a vacuum very similar to those found by DFT-B3LYP ab-initio methods. The atomic charge distribution of the dye molecule was obtained from DFT calculations, using the B3LYP hybrid functional and the ESP charge calculation method, setting the total net charge to +1. The positive charge of the LDS 722 molecules was compensated by the incorporation of one Mg^{+2} ion in isomorphic substitution of Al^{+3}. Framework charges were kept fixed to –1.2, 3.4, 1.4 and 0.4 for O, P, Al and Mg, respectively. Supercells consisting in 1x1x4 primary unit cells systems for both AFI and AEL (with primary unit cells of $Al_{12}P_{12}O_{48}$ and $Al_{20}P_{20}O_{80}$, respectively) frameworks were used for the calculations; both supercells were large enough as to host the isolated LDS 722 molecules while preventing computational artefacts.

The 1x1x4 supercells were initially optimized with the GULP code[39]. In the AFI framework, there is only one unique crystallographic position where Mg can replace Al. In contrast, three different T positions are available in the AEL framework, and the three of them were geometry-optimized (Figure S3 in the Supporting Information). Once obtained these frameworks, their coordinates were kept fixed in the calculations involving the LDS 722 molecules and the CVFF forcefield.

LDS 722 molecules were manually docked within the nanoporous structures; not only the trans-trans LDS 722 isomer was studied, but also isomers where some of the double-bonds were in cis configuration (cis1 and cis2) (see Figure S4 in the Supporting Information). The most stable location for the LDS 722 molecules was obtained by simulated annealing.

Interaction energies were calculated by subtracting the energy of the molecules in vacuo to the total energy of the system; all the energy values are given in kcal/mol per LDS 722 molecule.

Once obtained the most stable location of the LDS 722 molecules, the conformational flexibility in a vacuum or inside the different MgAPO frameworks was studied by NVT Molecular Dynamics (MD) simulations (at 298 K). Deviation of the planarity of the two aromatic rings was analyzed by calculating 'torsion' angle distributions between two atoms of one ring and two of the other ring, while rotation of the C-N bond in the aniline ring was analyzed by calculating the torsion angle distribution of the corresponding bond during the MD simulations.

Acknowledgements

The authors thank the Spanish Ministry of Economy and Innovation MINECO (MAT 2014-51937-C3-3 and MAT2012-31127) and Basque Government (IT339-10 and IT912-16) for funding this research. VMM and LGH acknowledge Ministerio de Economía y Competitividad MINECO for 'Ramón y Cajal' (RYC-2011-09505 and RYC-2012-11794, respectively) contracts and RSL acknowledges Universidad del País Vasco (UPV-EHU) for a predoctoral contract. Centro Técnico Informático-CSIC is acknowledged for running the calculations, and Accelrys for providing the computational software.

Keywords: AEL structure • NLO dye • crystallization inclusion method • molecular modeling • SHG

[1] D. N. Nikogosyan, *Nonlinear optical crystals: A complete survey* (Ed.: Springer Science & Business Media), Springer-Science: New York, 2005.

[2] J. Yu, Y. Cui, C. Wu, Y. Yang, Z. Wang, M. O'Keeffe, B. Chen, G. Qian, *Angew. Chemie - Int. Ed.* **2012**, *51*, 10542-10545.

[3] a) W. Wu, R. Tang, Q. Li, Z. Li, *Chem. Soc. Rev.* **2015**, *44*, 3997-4022; b) Z. Li, Q. Li, J. Qin, *Polym. Chem.* **2011**, *2*, 2723-2740; c) S. S. Sonawane, S. J. Nandre, R. R. Ahire, S. J. Shitole, *Pharma Chem.* **2014**, *6*, 33-38; d) S. Sagadevan, R. Varatharajan, *Mater. Phys. Mech.* **2013**, *18*, 11-17; e) S. Suresh, D. Arivuoli, *Rev. Adv. Mater. Sci.* **2012**, *30*, 243-253.

[4] S. Cambré, J. Campo, C. Beirnaert, C. Verlackt, P. Cool, W. Wenseleers, *Nat. Nanotechnol.* **2015**, *10*, 248-252.

[5] a) I. Chung, M. G. Kanatzidis, *Chem. Mater.* **2014**, *26*, 849-869; b) W. Yao, R. He, X. Wang, Z. Lin, C. Chen, *Adv. Opt. Mater.* **2014**, *2*, 411-417.

[6] C. Wang, T. Zhang, W. Lin, *Chem. Rev.* **2012**, *112*, 1084-1104.

[7] a) L. Li, J. Ge, H. Wu, Q. H. Xu, S. Q. Yao, *J. Am. Chem. Soc.* **2012**, *134*, 12157-12167; b) E. M. Boreham, L. Jones, A. N. Swinburne, M. Blanchard-Desce, V. Hugues, C. Terryn, F. Miomandre, G. Lemercier, L. S. Natrajan, *Dalt. Trans.* **2015**, *44*, 16127-16135.

[8] a) P. N. Prasad, D. J. Williams, *Introduction to nonlinear optical effects in molecules and polymers* (Eds.: J. Klafter, J. M. Drake), John Wiley & Sons, Inc.: New York, 1991; b) S. Wan, In *New Developments in Crystal Growth Research* (Ed.: G. V. Karas), Nova Science Publishers, Inc.: New York, 2005.

[9] a) C. V. McLaughlin, L. M. Hayden, B. Polishak, S. Huang, J. Luo, T. D. Kim, A. K. Y. Jen, *Appl. Phys. Lett.* **2008**, *92*, 1-4; b) M. Hochberg, T. Baehr-Jones, G. Wang, M. Shearn, K. Harvard, J. Luo, B. Chen, Z. Shi, R. Lawson, P. Sullivan, A. K. Y. Jen, L. Dalton, A. Scherer, *Nat. Mater.* **2006**, *5*, 703-709; c) W. R. Donaldson, C. L. Tang, *Appl. Phys. Lett.* **1984**, *44*, 25-27.

[10] G. S. He, L. S. Tan, Q. Zheng, P. N. Prasad, *Chem. Rev.* **2008**, *108*, 1245-1330.

[11] a) Z. Csók, P. Szuroczki, L. Kollár, H. M. Ngo, I. Ledoux-Rak, N. A. M. S. Caturello, R. Q. Albuquerque, *J. Phys. Chem. C* **2015**, *119*, 12608-12615; b) S. R. Marder, J. W. Perry, W. P. Schaefer, *Science* **1989**, *245*, 626-634; c) M. Ronchi, M. Pizzotti, A. O. Biroli, S. Righetto, R. Ugo, P. Mussini, M. Cavazzini, E. Lucenti, M. Salsa, P. Fantucci, *J. Phys. Chem. C* **2009**, *113*, 2745-2760; d) D. S. Chemla, J. Zyss, *Nonlinear Optical Properties of Organic Molecules and Crystals* (Ed.: D. S. Chemla), Academic Press: New York, 1987.

[12] a) Z. Li, W. Wu, Q. Li, G. Yu, L. Xiao, Y. Liu, C. Ye, J. Qin, Z. Li, *Angew. Chem. Int. Ed. Engl.* **2010**, *49*, 2763-2767; b) Y. Liao, S. Bhattacharjee, K. a. Firestone, B. E. Eichinger, R. Paranji, C. a. Anderson, B. H. Robinson, P. J. Reid, L. R. Dalton, *J. Am. Chem. Soc.* **2006**, *128*, 6847-6853.

[13] a) M. Rutkis, A. Jurgis, In *SPIE*; 2013; 8622, 86220R-1-86220R-11; b) P. a Sullivan, L. R. Dalton, *Acc. Chem. Res.* **2010**, *43*, 10-18.

[14] a) E. H. Kang, P. Jin, Y. Yang, J. Sun, J. Shen, *Chem. Commun.* **2006**, *1*, 4332-4334; b) A. Facchetti, A. Abbotto, L. Beverina, M. E. van der Boom, P. Dutta, G. Evmenenko, G. A. Pagani, T. J. Marks, *Chem. Mater.* **2003**, *15*, 1064-1072.

[15] H. Zhao, Y. H. Li, X.-S. Wang, Z.-R. Qu, L. Z. Wang, R. G. Xiong, B. F. Abrahams, Z. Xue, *Chem. - A Eur. J.* **2004**, *10*, 2386-2390.

[16] a) H. Zhao, Z. R. Qu, H. Y. Ye, R. G. Xiong, *Chem. Soc. Rev.* **2008**, *37*, 84-100; b) J. D. Lin, S. T. Wu, Z. H. Li, S. W. Du, *Dalt. Trans.* **2010**, *39*, 10719-10728.

[17] J. D. Lin, X. F. Long, P. Lin, S. W. Du, *Cryst. Growth Des.* **2010**, *10*, 146-157.

[18] J. Yu, Y. Cui, H. Xu, Y. Yang, Z. Wang, B. Chen, G. Qian, *Nat. Commun.* **2013**, *4*, 2719-2725.

[19] a) K. Hoffman, F. Marlow, In *Handbook of Zeolite Science and Technology* (Eds.: S. M. Auerbach, K. A. Carrado, P. K. Dutta), Marcel Dekker: New York, 2003; b) D. Brühwiler, G. Calzaferri, *Microporous Mesoporous Mater.* **2004**, *72*, 1-23; c) G. Calzaferri, *Langmuir* **2012**, *28*, 6216-6231; d) Z. Li, G. Luppi, A. Geiger, H. P. Josel, L. De Cola, *small* **2011**, *7*, 3193-3201.

[20] V. Martínez-Martínez, R. García, L. Gómez-Hortigüela, J. Pérez-Pariente, I. López-Arbeloa, *Chem. - A Eur. J.* **2013**, *19*, 9859-9865.

[21] L. Gartzia-Rivero, J. Bañuelos-Prieto, V. Martínez-Martínez, I. López-Arbeloa, *Chempluschem* **2012**, *77*, 61-70.

[22] R. García, V. Martínez-Martínez, R. Sola Llano, I. López-Arbeloa, J. Pérez-Pariente, *J. Phys. Chem. C* **2013**, *117*, 24063-24070.

[23] a) A. Devaux, G. Calzaferri, P. Belser, P. Cao, D. Bru, A. Kunzmann, *J. Mater. Chem.* **2014**, *26*, 6878-6885; b) H. Manzano, L. Gartzia-Rivero, J. Bañuelos, I. López-Arbeloa, *J. Phys. Chem. C* **2013**, *117*, 13331-13336.

[24] U. Vietze, O. Krauß, F. Laeri, G. Ihlein, F. Schüth, B. Limburg, M. Abraham, *Phys. Rev. Lett.* **1998**, *81*, 4628-4631.

[25] L. Benmohammadi, A. Erodabasi, K. Kock, F. Laeri, N. Owschimikow, U. Vietze, G. Ihlein, F. Schüth, O. Weiss, I. Braun, *Host-Guest-Systems based on Nanoporous Crystals* (Ed.: F. Laeri), John Wiley & Sons, Inc., 2003.

[26] a) G. Ihlein, F. Schüth, O. Krauβ, U. Vietze, F. Laeri, *Adv. Mater.* **1998**, *10*, 1117-1119; b) I. Braun, G. Ihlein, F. Laeri, J.U. Nöckel, G. Schulz-Ekloff, F. Schüth, U. Vietze, Ö. Weiss, D. Wöhrle, *Appl. Phys. B* **2000**, *70*, 335-343.

[27] J. Caro, G. Finger, J. Kornatowski, J. Richter-Mendau, L. Werner, B. Zibrowius, *Adv. Mater.* **1992**, *4*, 273-276.

[28] a) S. Cox, T. Gier, G. Stucky, *Chem. Mater.* **1990**, *2*, 609-619; b) G. A. Ozin, A. Kuperman, A. Stein, *Angew. Chem. Int. Ed. Engl.* **1989**, *28*, 359-376.

[29] a) R. Takenawa, Y. Komori, S. Hayashi, J. Kawamata, K. Kuroda, Chem. Mater. 2001, 13, 3741-3746; b) H. S. Kim, S. M. Lee, K. Ha, C. Jung, Y. J. Lee, Y. S. Chun, D. Kim, B. K. Rhee, K. B. Yoon, J. Am. Chem. Soc. 2004, 126, 673-682; c) J. Caro, F. Marlow, M. Wübbenhorst, *Adv. Mater.* **1994**, 413-416; d) S. D. Cox, T. E. Gier, G. D. Stucky, J. Bierlein, *J. Am. Chem. Soc.* **1988**, *110*, 2986-2987.

[30] a) X.M. Duan, H. Konami, S. Okada, H. Oikawa, H. Matsuda, H. Nakanishi, *J. Phys. Chem.* **1996**, *100*, 17780-17785; b) D. Seth, S. Sarkar, R. Pramanik, C. Ghatak, P. Setua, N. Sarkar, *J. Phys. Chem. B* **2009**, *113*, 6826-6833.

[31] L. Cerdán, a. Costela, I. García-Moreno, J. Bañuelos, I. López-Arbeloa, *Laser Phys. Lett.* **2012**, *426*, 426-433.

[32] a) E. Abraham, C. Grauby-Heywang, S. Selector, G. Jonusauskas, *J. Photochem. Photobiol. B.* **2008**, *93*, 44-52; b) A. Mishra, S. Sahu, S. Tripathi, G. Krishnamoorthy, *Photochem. Photobiol. Sci.* **2014**, *137*, 9-14; c) Y. Huang, T. Cheng, F. Li, C. H. Huang, S. Wang, W. Huang, Q. Gong, *J. Phys. Chem. B* **2002**, *106*, 10041-10050; d) W. Rettig, *Angew. Chem. Int. Ed. Engl.* **1986**, *25*, 971-988.

[33] V. Martínez-Martínez, R. García, L. Gómez-Hortigüela, R. Sola Llano, J. Pérez-Pariente, I. López-Arbeloa, *ACS Photonics* **2014**, *1*, 205-211.

[34] J. Zhao, K. Oniwa, A. Islam, C. Qin, N. Asao, L. Han, Y. Yamamoto, T. Jin, *Org. Chem. Front.* **2015**, *2*, 253-258.

[35] K.P. Schröder, J. Sauer, M. Leslie, C. Richard, A. Catlow, J. M. Thomas, *Chem. Phys. Lett.* **1992**, *188*, 320-325.

[36] S. Inoué, O. Shimomura, M. Goda, M. Shribak, P. T. Tran, *Proc. Natl. Acad. Sci. U. S. A.* **2002**, *99*, 4272-4277.

[37] Forcite module, Material Studio. Accelrys Inc.: San Diego, CA **2013**.

[38] P. Dauber-Osguthorpe, V. a Roberts, D. J. Osguthorpe, J. Wolff, M. Genest, a T. Hagler, *Proteins* **1988**, *4*, 31-47.

[39] J. D. Gale, A. L. Rohl, *Mol. Simul.* **2003**, *29*, 291-341.